Feshbach resonances in ultracold ^{85}Rb

Caroline L. Blackley, C. Ruth Le Sueur, and Jeremy M. Hutson
Joint Quantum Centre (JQC) Durham/Newcastle, Department of Chemistry, Durham University, South Road, Durham, DH1 3LE, United Kingdom

Daniel J. McCarron, Michael P. Köppinger, Hung-Wen Cho, Daniel L. Jenkin, and Simon L. Cornish
Joint Quantum Centre (JQC) Durham/Newcastle, Department of Physics, Durham University, South Road, Durham DH1 3LE, United Kingdom

(Received 21 December 2012; published 7 March 2013)

We present 17 experimentally confirmed Feshbach resonances in optically trapped ^{85}Rb. Seven of the resonances are in the ground-state channel $(f,m_f) = (2,+2) + (2,+2)$ and nine are in the excited-state channel $(2,-2) + (2,-2)$. We find a wide resonance at high field in each of the two channels, offering possibilities for the formation of larger ^{85}Rb condensates and studies of few-body physics. A detailed coupled-channel analysis is presented to characterize the resonances and also provides an understanding of the inelastic losses observed in the excited-state channel. In addition we have confirmed the existence of one narrow resonance in a $(2,+2) + (3,+3)$ spin mixture.

DOI: 10.1103/PhysRevA.87.033611 PACS number(s): 67.85.−d, 31.50.Bc, 34.20.Cf

I. INTRODUCTION

The creation of ultracold molecules is currently of great interest. They offer a wide range of applications including studies of few-body quantum physics, high-precision spectroscopy, quantum simulators for many-body phenomena, and controlled chemistry [1,2]. Ultracold molecules have a far richer substructure than atoms and so molecular condensates with tunable interactions offer unique levels of control over collision properties [3]. One route to ultracold molecules is through the association of two ultracold atoms into a weakly bound molecule [4]. This is achieved by sweeping the magnetic field adiabatically across a Feshbach resonance such that energy of the separated atomic states is tuned adiabatically through an avoided crossing with the energy of a weakly bound molecular state [3]. The molecules can then be transferred into their rovibrational ground state by stimulated Raman adiabatic passage (STIRAP). This method has been used effectively in several systems to create ultracold molecules [5–7].

^{85}Rb is a promising species for ultracold atomic gas experiments, though it has often been overlooked due to the challenges of forming a Bose-Einstein condensate (BEC) [8,9]. Our recent work shows the benefits of ^{85}Rb for RbCs production [10]. However, for these experiments a full understanding of the scattering behavior of ^{85}Rb is required. Most previous work on ^{85}Rb has focused on the wide resonance near 155 G in the $(f,m_f) = (2,-2) + (2,-2)$ channel [11]. This resonance is suitable for experiments that require precise tuning of the scattering length and has been used extensively in studies of condensate collapse [9,12–14], the formation of bright matter wave solitons [15], and few-body physics [16]. Further work using ^{85}Rb includes spectroscopic studies of photoassociation [17,18] and measurements of inelastic collision rates [19,20], molecular binding energies [21], molecule formation [22–26], and Efimov states [14,16,27]. Despite extensive work in this region of the $(2,-2) + (2,-2)$ channel, there appears to have been little theoretical or experimental work on the ground state or at higher field.

In this paper we reveal the rich Feshbach structure of ^{85}Rb. We use coupled-channel calculations to predict Feshbach resonances in both the $(2,-2) + (2,-2)$ channel (designated ee) and the $(2,+2) + (2,+2)$ channel (designated aa) and confirm 16 of them experimentally. In addition we identify a resonance in the mixed spin channel $(2,+2) + (3,+3)$. The structure of the paper is as follows: Sec. II describes the theory and calculations; Sec. III describes the experimental setup and methodology; Sec. IV describes the results; and in Sec. V we conclude with an outlook on future research prospects.

II. THEORY

The collision Hamiltonian for a pair of alkali-metal atoms is

$$\frac{\hbar^2}{2\mu}\left[-r^{-1}\frac{d^2}{dr^2}r + \frac{\hat{L}^2}{r^2}\right] + \hat{H}_1 + \hat{H}_2 + \hat{V}(r), \qquad (1)$$

where r is the internuclear distance, μ is the reduced mass, $\hat{L}$ is the rotational angular momentum operator, and $\hat{V}$ is the interaction operator. $\hat{H}_1$ and $\hat{H}_2$ are the monomer Hamiltonians of the free atoms,

$$\hat{H}_i = \zeta_i \hat{i}_i \cdot \hat{s}_i + (g_e \mu_B \hat{s}_{iz} + g_n \mu_B \hat{i}_{iz})B, \qquad (2)$$

where ζ_i is the hyperfine coupling constant of atom i, g_e and g_n are the electron and nuclear g factors, $\hat{s}$ and $\hat{i}$ are the electron and nuclear spin operators, and B is the magnetic field.

The calculations in the present paper are carried out in two different basis sets: a fully decoupled basis set

$$|s_{Rb} m_{sRb}\rangle\, |i_{Rb} m_{iRb}\rangle\, |s_{Rb} m_{sRb}\rangle\, |i_{Rb} m_{iRb}\rangle\, |L M_L\rangle$$

and a partly coupled basis set

$$|f_a, m_{f,a}\rangle\, |f_b, m_{f,b}\rangle\, |F, M_F\rangle\, |L, M_L\rangle.$$

The two basis sets give identical bound-state energies and scattering properties, but different views of the bound-state wave functions. In both cases the basis sets are symmetrized to take account of identical particle symmetry. The resulting coupled equations are diagonal in the total projection number $M_{tot} = M_F + M_L$, where $M_F = m_{f,a} + m_{f,b} = m_{sRb_a} + m_{iRb_a} + m_{sRb_b} + m_{iRb_b}$. The basis sets used include all functions with $L = 0$ and 2 for the required value of M_{tot}, which

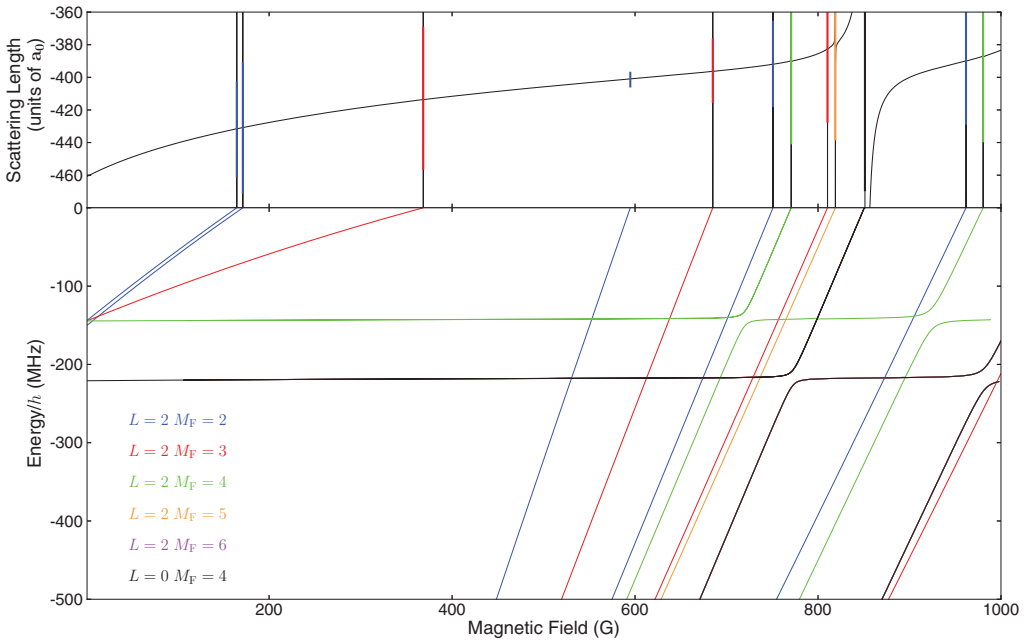

FIG. 1. (Color online) Top panel: Calculated s-wave scattering length in the aa channel of $^{85}Rb_2$, with resonances marked with lines whose color depends on their M_F value (see legend); the length of each line is proportional to the logarithm of the width of the resonance. Bottom panel: Energies of weakly bound molecular states, relative to the aa threshold, (2,+2) + (2,+2) channel. All calculations in this figure are for $M_{\rm tot} = 4$, corresponding to s-wave scattering in the aa channel.

for s-wave scattering is equal to $m_{f,a} + m_{f,b}$ for the incoming channel.

The coupled-channel scattering calculations are performed using the MOLSCAT program [28], as modified to handle collisions in an external field [29]. Calculations are carried out with a fixed-step log-derivative propagator [30] from 0.3 to 2.1 nm and a variable-step Airy propagator [31] from 2.1 to 1500 nm. The wave functions are matched to their long-range solutions, the Ricatti-Bessel functions, at 1500 nm to find the S-matrix elements. The s-wave ($L = 0$) scattering length $a(k)$ is then obtained from the identity $a(k) = (ik)^{-1}(1 - S_{00})/(1 + S_{00})$ [32], where S_{00} is the diagonal S-matrix element in the incoming channel and k is the wave vector. The bound-state calculations use the BOUND [33] and FIELD [34] packages, which locate bound states as described in Ref. [35]. BOUND and FIELD use propagator methods, without radial basis sets. The calculations allow the assignment of quantum numbers to the states responsible for resonances in the scattering length.

The scattering and bound-state calculations are carried out using the potential curves and magnetic dipole coupling function from Ref. [36]. The potentials were obtained by fitting to spectroscopic data on both the singlet [37] and triplet states of $^{87}Rb_2$ and the triplet state of $^{85}Rb_2$, together with several Feshbach resonances in $^{87}Rb_2$, $^{87}Rb^{85}Rb$, and $^{85}Rb_2$. The singlet and triplet scattering lengths for ^{85}Rb on the potentials of Ref. [36] are $a_S = 2735\ a_0$ and $a_T = -386\ a_0$, respectively.

The calculated s-wave scattering length for the aa channel is shown in the top panel of Fig. 1 and the binding energies of the near-threshold molecular states responsible for the resonances are shown in the bottom panel. The resonance positions are given in Table I, along with their widths Δ as defined by local fits to the standard formula $a(B) = a_{\rm bg}\,[1 - \Delta/(B - B_0)]$ [38], where $a_{\rm bg}$ is the background scattering length, Δ is the width, and B_0 is the position of the pole in the scattering length. Quantum numbers were assigned by carrying out approximate calculations with either M_F or F and M_F restricted to specific values. For a homonuclear diatomic molecule, F is a nearly good quantum number in the low-field region where the free-atom energies vary linearly with B. Figure 1 shows one wide resonance near 851 G ($\Delta = 1.2$ G) that offers attractive possibilities for precise tuning of the scattering length and many narrower resonances that may be useful for molecule formation.

For an excited-state channel, where inelastic scattering can occur, the scattering length $a(B)$ is complex, $a(B) = \alpha(B) - i\beta(B)$. The two-body inelastic loss rate is proportional to $\beta(B)$. The top two panels of Fig. 2 show the real and imaginary parts of $a(B)$ for s-wave collisions in the ee channel. In this case the inelastic collisions produce atoms in lower magnetic sublevels, with $m_{f,a}$ and/or $m_{f,b} > -2$. The bottom panel shows the corresponding molecular bound states for $M_F = -4$, -5, and -6, obtained from calculations with M_F fixed. We also carried out calculations of the quasibound states with $M_F = -2$ and -3 near the ee threshold in order to identify the states responsible for the remaining resonances. These calculations use the FIELD program with propagation to reduced distances around 100 nm in order to reduce interference from continuum states.

In the presence of inelastic scattering, $a(B)$ does not show actual poles at resonance [32]. If the background inelastic scattering is negligible, the real part $\alpha(B)$ shows an oscillation of amplitude $a_{\rm res}$, while the imaginary part shows a peak of height $a_{\rm res}$. The resonant scattering length $a_{\rm res}$ is determined

TABLE I. Location and assignment of Feshbach resonances for $^{85}Rb_2$ in the aa channel in the field range between 0 and 1000 G. All quantum numbers in the table refer to the molecular states. The experimental errors shown are statistical uncertainties resulting from the fits as described in the text. Additional systematic uncertainties of 0.1 and 0.5 G apply to resonance positions in the field ranges 0 to 400 and 400 to 1000 G, respectively.

Incoming s-wave $(2,+2)+(2,+2)$ state								
Experiment		Theory						
		Assignment						a_{bg}
B_0 (G)	δ(G)	L	(f_a,f_b)	F	M_F	B_0 (G)	Δ (mG)	(bohr)
164.74(1)	0.08(2)	2	(2,2)	4	2	164.7	−0.0006	−432
171.36(1)	0.12(2)	2	(2,2)	2	2	171.3	−0.02	−431
368.78(4)	0.4(1)	2	(2,2)	4	3	368.5	−0.06	−413
		2	(2,3)	3	2	594.9	-0.4×10^{-6}	−401
		2	(2,3)	5	3	685.0	-0.4×10^{-4}	−396
		2	(2,3)	5	2	750.8	−0.0003	−392
770.81(1)	0.11(2)	2	(2,3)	5	4	770.7	−0.5	−390
809.65(3)	0.3(1)	2	(2,3)	3	3	809.7	−0.09	−383
819.8(2)	0.7(5)	2	(2,3)	5	5	819.0	−5.4	−380
852.3(3)	1.3(4)[a]	0	(2,3)	5	4	851.3	−1199	−393
		2	(2,3)	2	2	961.8	−0.01	−390
		2	(2,3)	4	4	980.5	−0.7	−387

[a]Experimental width determined from the difference between the minima and maxima in the measured atom number.

by the *ratio* of the couplings from the quasibound state responsible for the resonance to the incoming and inelastic channels [32]. If there is significant background scattering, then there is a more complicated asymmetric line shape that may show a substantial dip in the inelastic scattering near resonance [39]. Figure 2 shows resonances of all these different types: The resonances due to bound states with $M_F = m_{f,a} + m_{f,b} = -4, -5$, and -6 are polelike, with values of at least $a_{res} > 20\ a_0$ and with most having $a_{res} > 1000\ a_0$. These resonances produce pronounced features in $\alpha(B)$ and sharp

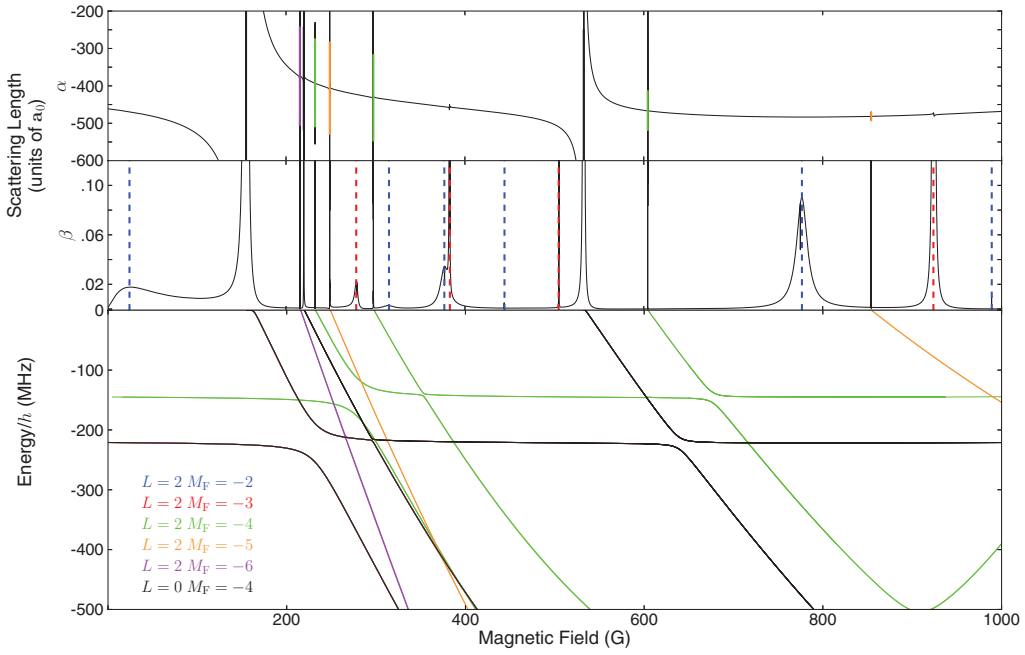

FIG. 2. (Color online) Top two panels: Real and imaginary parts of the s-wave scattering length in the ee channel of $^{85}Rb_2$. Each resonance is indicated by a colored vertical line that indicates its M_F value (see legend); for polelike resonances, the length of the line is proportional to the logarithm of the width of the resonance. Inelastically dominated resonances are not always evident in α, but appear as peaks in β and are indicated by dashed vertical lines. Bottom panel: Energies of weakly bound molecular states, relative to the ee threshold, $(2,-2)+(2,-2)$ channel. Only states with no continuum interference ($M_F \leqslant -4$) are shown in the bound-state map, but all resonances are included in the scattering length. All calculations in this figure are for $M_{tot} = -4$, corresponding to s-wave scattering in the ee channel.

TABLE II. Location and assignment of Feshbach resonances for $^{85}Rb_2$ in the ee channel in the field range between 0 and 1000 G. All resonances shown satisfy $a_{res} \geqslant 1\ a_0$. All quantum numbers in the table refer to the molecular states. The experimental errors shown are statistical uncertainties resulting from the fits as described in the text. Additional systematic uncertainties of 0.1 and 0.5 G apply to resonance positions in the field ranges 0 to 400 and 400 to 1000 G, respectively. The resonances near 155 and 220 G have been measured previously [21,44].

Incoming s-wave $(2,-2)+(2,-2)$ state							
Experiment		Theory					
		Assignment				a_{res}	a_{bg}
B_0 (G)	δ (G)	L	M_F	B_0 (G)	Δ (mG)	(bohr)	(bohr)
156(1)	10.5(5)	0	−4	155.3	10900	$\geqslant$10000	−441
		2	−6	215.5	5.5	4000	−374
219.58(1)	0.22(9)	0	−4	219.9	9.1	4000	−379
232.25(1)	0.23(1)	2	−4	232.5	2.0	400	−393
248.64(1)	0.12(2)	2	−5	248.9	2.9	5000	−406
297.42(1)	0.09(1)	2	−4	297.7	1.8	5000	−432
382.36(2)	0.19(1)	2	−3	382		15	−457
532.3(3)	3.2(1)[a]	0	−4	532.9	2300	$\geqslant$10000	−474
604.1(1)	0.2(1)	2	−4	604.4	0.03	700	−466
		2	−5	854.3	0.002	25	−481
924.52(4)	2.8(1)	2	−3	924		9	−476

[a]Experimental width determined from the difference between the minima and maxima in the measured atom number.

peaks in $\beta(B)$, off scale in Fig. 2. By contrast, resonances due to states with $M_F = -2$ and -3 show much weaker features with $a_{res} < 15\ a_0$ and some lower than $0.01\ a_0$. These are barely perceptible in $\alpha(B)$ on the scale of Fig. 2 and produce broader, weaker peaks in $\beta(B)$. The distinction occurs because all the inelastic channels have $M_F > -4$: Bound states with $M_F = -2$ and -3 are generally more strongly coupled to inelastic channels with the same M_F than to the incoming channel with $M_F = -4$, whereas the reverse is true for bound states with $M_F = -4$, -5, and -6. Many of the features show quite pronounced asymmetry in the shape of the inelastic peaks. All of the resonances with $a_{res} > 1.0\ a_0$ are listed in Table II along with their widths and approximate a_{res} values.

We have also investigated the scattering length for mixed spin channels with a view to identify broad resonances suitable for manipulating interactions. Most channels exhibit strong inelastic decay with measured trap lifetimes of ∼100 ms. However, the $(2,+2)+(3,+3)$ channel is immune to inelastic spin exchange collisions, resulting in trap lifetimes of ∼5 s. The scattering length in the mixed spin channel $(2,+2)+(3,+3)$ shows two polelike resonances at 818.8 and 909.9 G, both with widths of 2 mG, and $a_{res} = 1600\ a_0$ and $800\ a_0$, respectively.

III. EXPERIMENT

The details of our apparatus and cooling scheme are presented in Refs. [10,40,41] and are only briefly recounted here. Ultracold samples of ^{85}Rb are collected in a magneto-optical trap before being optically pumped into the $(2,-2)$ state and loaded into a magnetic quadrupole trap. Forced rf evaporation cools the ^{85}Rb atoms to 50 μK, where further efficient evaporation is impeded by Majorana losses [42]. The atoms are then transferred into a crossed dipole trap derived from a single-mode 1550-nm 30-W fiber laser. When loading, the power in each beam is set to 4 W, creating a trap 100 μK deep with radial and axial trap frequencies of 455 and 90 Hz, respectively. After loading, when performing Feshbach spectroscopy in the absolute internal ground state, the ^{85}Rb atoms are transferred into the $|2,+2\rangle$ state by rf adiabatic passage [43]. A vertical magnetic field gradient of 21.2 G/cm is then applied, slightly below the 22.4 G/cm necessary to levitate ^{85}Rb. However, for our present coil configuration this gradient adds to, rather than cancels, gravity when working with the $(2,-2)$ state. In this case, therefore, no magnetic field gradient is applied and the atoms are confined in a purely optical potential.

A typical experiment begins with $6.0(3) \times 10^5$ ^{85}Rb atoms at 10.2(1) μK confined in the dipole trap in either $(2,+2)$ or $(2,-2)$. To perform Feshbach spectroscopy, the magnetic field is switched to a specific value in the range 0 to 1000 G. Evaporative cooling is then performed by reducing the dipole beam powers by a factor of 4 over 2 s. The atomic sample is then held for 1 s in this final potential. Resonant absorption imaging is used to probe the atoms after each experimental cycle. Feshbach resonances are identified by examining the variation in the atom number and temperature as a function of the magnetic field. The magnetic field is calibrated using microwave spectroscopy between the hyperfine states of ^{85}Rb. These measurements reveal the long-term reproducibility of the field to be 0.1 G for the range 0 to 400 G and 0.5 G for the range 400 to 1000 G.

To perform Feshbach spectroscopy on a spin mixture of $(2,+2)+(3,+3)$, a cloud of $(2,+2)$ atoms is first cooled using the same evaporation sequence as above at 22.6 G. To populate the $(3,+3)$ state a microwave pulse is applied for 250 ms at 3.0887 GHz, producing a mixture containing $7(1) \times 10^4$ atoms in each of the $(2,+2)$ and $(3,+3)$ spin states. The magnetic field is then switched to a value in the range 0 to 1000 G and held for 750 ms. Finally, Stern-Gerlach spectroscopy and absorption imaging are used to probe both spin states simultaneously.

IV. EXPERIMENTAL RESULTS

We have observed seven resonances in the aa channel and nine resonances in the ee channel. The observed and predicted resonance positions and widths are listed in Tables I and II and show good agreement between experiment and theory. In the ground state, all the widest calculated resonances are seen experimentally, with the exception of the two high-field resonances where the experimental field is less reproducible. In the excited state, all but two of the predicted polelike resonances are seen, together with two of the inelastically dominated features.

Figure 3 shows fine scans of the atom number for two of the narrow resonances, one in each of the aa and ee channels. Such resonances produce sharp drops in atom number. In the aa channel the drop in atom number is due to the three-body recombination rate, which scales as a^4 [3], whereas in the ee channel the loss is due to both three-body and two-body processes, which are discussed below. As these mechanisms are density dependent there is a concomitant heating of the cloud observed. The experimental positions and widths of these resonances are determined by fitting a Lorentzian, with width δ, to the data points. The value of δ is set by a combination of field stability, field spread due to the magnetic gradient, and experimental sequence, i.e., how long the atomic sample is held at each magnetic field. It should be noted that the experimental and theoretical widths are entirely different quantities for narrow resonances and should not be compared.

There are three resonances with widths greater than 1 G. Figure 4 shows a fine scan across the resonances near 530 G in the ee channel and 850 G in the aa channel. In these cases the atom number shows both a peak and a trough. The trough (loss maximum) again corresponds to the resonance position, while the peak (loss minimum) occurs near the zero crossing of the scattering length. The three wide resonances are several orders of magnitude wider than any of the other resonances seen and provide valuable control over the scattering length. Note that our measurement of the position of the well-known 155-G resonance in the ee channel is not as accurate as the determination from bound-state spectroscopy [21].

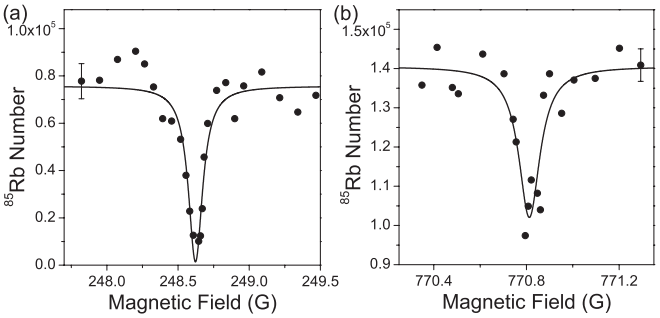

FIG. 3. Narrow resonances in ^{85}Rb, with fitted width $\delta < 0.2$ G, observed as loss features in the atom number due to an enhancement in inelastic collisions near the resonance. (a) A resonance in the $(2,-2)$ state at 248.64(1) G. (b) A resonance in the $(2,+2)$ state at 770.81(1) G. The error bars show the standard deviation for multiple control shots at specific magnetic fields.

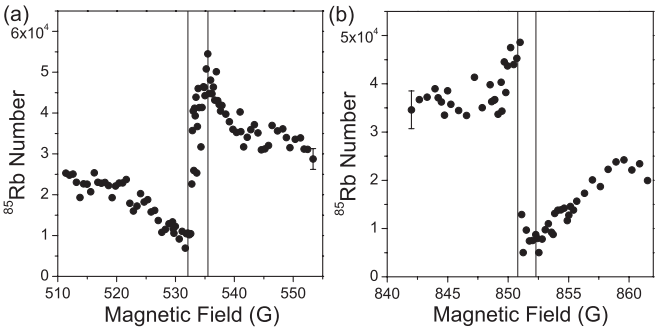

FIG. 4. Broad resonances in ^{85}Rb, with width $\Delta > 1$ G, observed as features in the atom number. (a) A resonance in the $(2,-2)$ state at 532.3(3) G. (b) A resonance in the $(2,+2)$ state at 852.3(3) G. The experimental widths are determined by the difference between the positions of the minima and maxima in the atom number marked with solid lines in both plots. The error bars show the standard deviation for multiple control shots at specific magnetic fields.

In the ee channel, the two inelastically dominated features that are seen experimentally are those with the largest $a_{\rm res}$ values. The number of atoms in the trap decreases around these resonances due to an increase in the two-body loss rate, as shown in Figs. 5(a) and 5(b). The inelastic collisions also

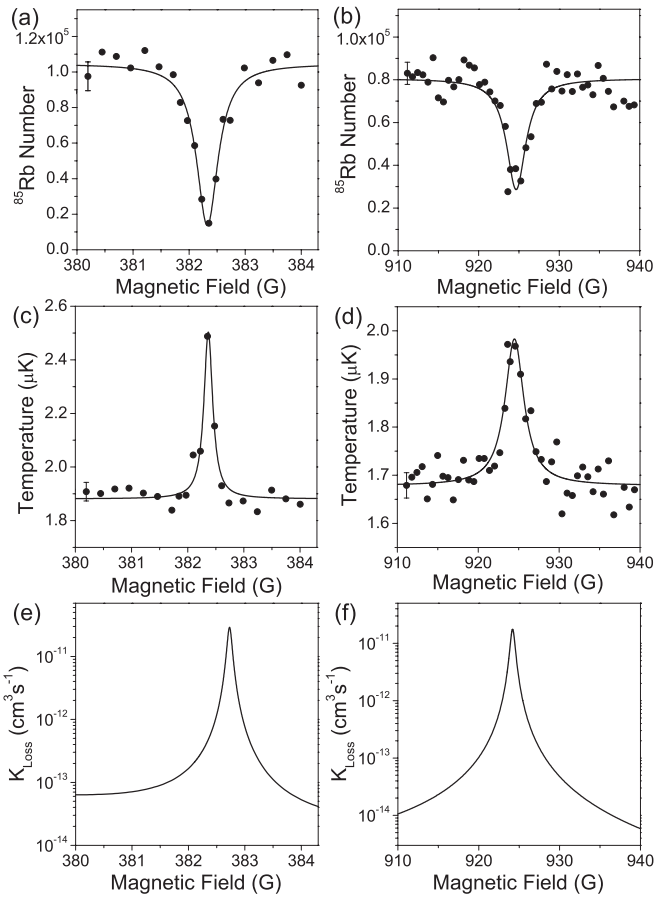

FIG. 5. The two inelastically dominated features observed in the $(2,-2)$ state. (a) and (b) show the atom number while (c) and (d) show temperature. Error bars show the standard deviation for multiple control shots at specific magnetic fields. (e) and (f) show the calculated rate coefficient for two-body loss $K_{\rm loss}$.

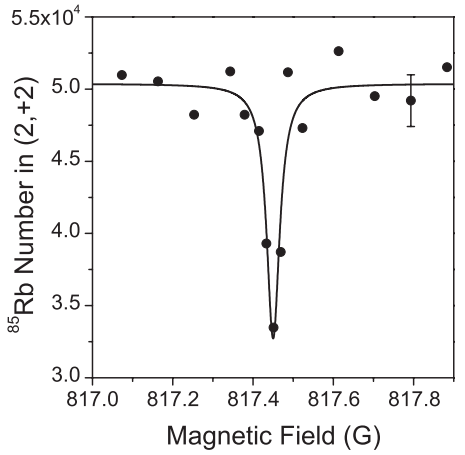

FIG. 6. Resonance measured between the (2,+2) and (3,+3) spin states in ^{85}Rb at 817.45(5) G. On resonance the increased inelastic collision rate in the mixture results in a loss feature in the (2,+2) atom number as a function of magnetic field. The error bars show the standard deviation for multiple control shots at a specific magnetic field.

lead to an increase in temperature, as shown in Figs. 5(c) and 5(d). The rate coefficient for two-body losses due to inelastic collisions from a channel n is

$$K^{(2)}_{\rm loss}(B) = \frac{2h}{\mu} g_n \beta(B), \tag{3}$$

where $\beta(B)$ is the imaginary part of the scattering length and $g_n = 2$ for a thermal cloud of identical bosons [3]. The calculated rate coefficients for the two resonances are shown in Figs. 5(e) and 5(f); they peak around 1×10^{-11} cm^3/s, which is an order of magnitude higher than for any of the other inelastically dominated features.

We have also measured one resonance in the (2,+2) + (3,+3) mixed spin channel. The experimental results are presented in Fig. 6, where a loss feature in the ^{85}Rb (2,+2) number reveals the location of the resonance. A Lorentzian fit gives a resonance position of 817.45(5) G and an experimental width of 0.031(1) G, which may be compared with the predicted position of 818.8 G.

V. CONCLUSION

A detailed understanding of the two-body scattering behavior is essential for understanding many phenomena in ultracold gases. These include studies of molecule formation [22–26], Efimov states and their universality [14,16,27,45], dimer collisions and few-body physics [46], BEC production [9,47], controlled condensate collapse [12–14], and the formation of bright matter wave solitons [15]. The scattering properties of many alkali-metal atoms have been documented in the literature [3]. However, nearly all previous work on ^{85}Rb has focused on a single broad resonance near 155 G. This paper redresses this balance by presenting a detailed study of the scattering properties of ^{85}Rb, revealing additional broad resonances and numerous unreported narrow resonances in both the ee and aa channels. As has been the case for other alkali-metal atoms, this work will facilitate many future studies using ^{85}Rb.

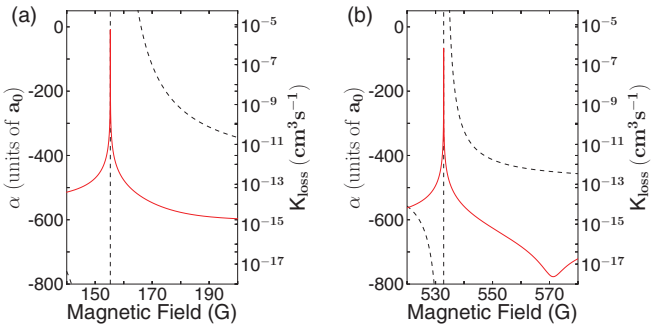

FIG. 7. (Color online) Rate coefficient for two-body loss $K_{\rm loss}$ (red solid lines), which is proportional to the imaginary part of the scattering length, and the corresponding real part of the scattering length (dashed lines) for the two resonances with $\Delta > 1$ G in the ee channel. Note the dip in $K_{\rm loss}$ on the high-field side of the 532 G resonance.

We have recently explored interspecies Feshbach resonances in mixtures of ^{85}Rb and ^{133}Cs [10] as a key step towards the production of ^{85}Rb^{133}Cs molecules. The improved understanding of the collisional behavior of ^{85}Rb resulting from the present work is essential for the production of the high phase-space density mixtures required for efficient molecule formation. In particular, the two broad resonances at higher magnetic field (851 G in the aa channel and 532 G in the ee channel) offer different magnetic field regions for evaporative cooling. The elastic to inelastic collision ratio in the vicinity of these features is potentially more favorable for evaporative cooling than near the 155-G resonance, where direct evaporation of ^{85}Rb to a BEC is possible [9,48]. Figure 7 compares the scattering properties around the 532-G resonance with those near the 155-G resonance. The results for the 532-G resonance show a pronounced dip in the rate coefficient for two-body loss near 570 G, due to interference between the resonant and background contributions to the inelastic scattering [32,39], which offers a range of magnetic fields where more efficient cooling may be possible. No such dip in the two-body loss rate is present near the 155-G resonance. Alternatively, the aa channel offers the prospect of evaporative cooling free from two-body loss. Although the background scattering length is moderately large and negative for ground-state atoms (see Fig. 1), the broad resonance at 851 G may be used to tune the scattering length to modest positive values, improving the evaporation efficiency and offering the prospect of BEC formation directly in the absolute ground state. The improved knowledge of ^{85}Rb scattering presented in this paper, together with similar knowledge for ^{133}Cs [49,50], should make it possible to devise ways to cool ^{85}Rb-^{133}Cs mixtures to phase-space densities suitable for magnetoassociation, and thus bring ground-state ^{85}Rb^{133}Cs molecules within reach.

ACKNOWLEDGMENTS

We thank Paul S. Julienne for many valuable discussions and Eite Tiesinga for providing a subroutine for the Rb_2 potential curves. This work was supported by EPSRC and by EOARD Grant No. FA8655-10-1-3033. C.L.B. was supported by a Doctoral Fellowship from Durham University.

[1] L. D. Carr, D. DeMille, R. V. Krems, and J. Ye, New J. Phys. **11**, 055049 (2009).

[2] R. V. Krems, Int. Rev. Phys. Chem. **24**, 99 (2005).

[3] C. Chin, R. Grimm, E. Tiesinga, and P. S. Julienne, Rev. Mod. Phys. **82**, 1225 (2010).

[4] B. Damski, L. Santos, E. Tiemann, M. Lewenstein, S. Kotochigova, P. Julienne, and P. Zoller, Phys. Rev. Lett. **90**, 110401 (2003).

[5] K.-K. Ni, S. Ospelkaus, M. H. G. de Miranda, A. Pe'er, B. Neyenhuis, J. J. Zirbel, S. Kotochigova, P. S. Julienne, D. S. Jin, and J. Ye, Science **322**, 231 (2008).

[6] F. Lang, K. Winkler, C. Strauss, R. Grimm, and J. Hecker Denschlag, Phys. Rev. Lett. **101**, 133005 (2008).

[7] J. G. Danzl, M. J. Mark, E. Haller, M. Gustavsson, R. Hart, J. Aldegunde, J. M. Hutson, and H.-C. Nägerl, Nat. Phys. **6**, 265 (2010).

[8] J. P. Burke, J. L. Bohn, B. D. Esry, and C. H. Greene, Phys. Rev. Lett. **80**, 2097 (1998).

[9] S. L. Cornish, N. R. Claussen, J. L. Roberts, E. A. Cornell, and C. E. Wieman, Phys. Rev. Lett. **85**, 1795 (2000).

[10] H.-W. Cho, D. J. McCarron, M. P. Köppinger, D. L. Jenkin, K. L. Butler, P. S. Julienne, C. L. Blackley, C. R. Le Sueur, J. M. Hutson, and S. L. Cornish, Phys. Rev. A **87**, 010703(R) (2013).

[11] J. M. Vogels, C. C. Tsai, R. S. Freeland, S. J. J. M. F. Kokkelmans, B. J. Verhaar, and D. J. Heinzen, Phys. Rev. A **56**, R1067 (1997).

[12] J. L. Roberts, N. R. Claussen, S. L. Cornish, E. A. Donley, E. A. Cornell, and C. E. Wieman, Phys. Rev. Lett. **86**, 4211 (2001).

[13] E. A. Donley, N. R. Claussen, S. L. Cornish, J. L. Roberts, E. A. Cornell, and C. E. Wieman, Nature (London) **412**, 295 (2001).

[14] P. A. Altin, G. R. Dennis, G. D. McDonald, D. Döring, J. E. Debs, J. D. Close, C. M. Savage, and N. P. Robins, Phys. Rev. A **84**, 033632 (2011).

[15] S. L. Cornish, S. T. Thompson, and C. E. Wieman, Phys. Rev. Lett. **96**, 170401 (2006).

[16] R. J. Wild, P. Makotyn, J. M. Pino, E. A. Cornell, and D. S. Jin, Phys. Rev. Lett. **108**, 145305 (2012).

[17] C. C. Tsai, R. S. Freeland, J. M. Vogels, H. M. J. M. Boesten, B. J. Verhaar, and D. J. Heinzen, Phys. Rev. Lett. **79**, 1245 (1997).

[18] P. Courteille, R. S. Freeland, D. J. Heinzen, F. A. van Abeelen, and B. J. Verhaar, Phys. Rev. Lett. **81**, 69 (1998).

[19] J. L. Roberts, N. R. Claussen, S. L. Cornish, and C. E. Wieman, Phys. Rev. Lett. **85**, 728 (2000).

[20] J. L. Roberts, J. P. Burke, N. R. Claussen, S. L. Cornish, E. A. Donley, and C. E. Wieman, Phys. Rev. A **64**, 024702 (2001).

[21] N. R. Claussen, S. J. J. M. F. Kokkelmans, S. T. Thompson, E. A. Donley, E. Hodby, and C. E. Wieman, Phys. Rev. A **67**, 060701 (2003).

[22] E. A. Donley, N. R. Claussen, S. T. Thompson, and C. E. Wieman, Nature (London) **417**, 529 (2002).

[23] S. T. Thompson, E. Hodby, and C. E. Wieman, Phys. Rev. Lett. **95**, 190404 (2005).

[24] T. Köhler, E. Tiesinga, and P. S. Julienne, Phys. Rev. Lett. **94**, 020402 (2005).

[25] E. Hodby, S. T. Thompson, C. A. Regal, M. Greiner, A. C. Wilson, D. S. Jin, E. A. Cornell, and C. E. Wieman, Phys. Rev. Lett. **94**, 120402 (2005).

[26] B. L. Brown, A. J. Dicks, and I. A. Walmsley, Phys. Rev. Lett. **96**, 173002 (2006).

[27] M. Stoll and T. Köhler, Phys. Rev. A **72**, 022714 (2005).

[28] J. M. Hutson and S. Green, MOLSCAT computer program, version 14 (Collaborative Computational Project No. 6 of the UK Engineering and Physical Sciences Research Council, 1994).

[29] M. L. González-Martínez and J. M. Hutson, Phys. Rev. A **75**, 022702 (2007).

[30] D. E. Manolopoulos, J. Chem. Phys. **85**, 6425 (1986).

[31] M. H. Alexander, J. Chem. Phys. **81**, 4510 (1984).

[32] J. M. Hutson, New J. Phys. **9**, 152 (2007).

[33] J. M. Hutson, BOUND computer program, version 5 (Collaborative Computational Project No. 6 of the UK Engineering and Physical Sciences Research Council, 1993).

[34] J. M. Hutson, FIELD computer program, version 1 (2011).

[35] J. M. Hutson, E. Tiesinga, and P. S. Julienne, Phys. Rev. A **78**, 052703 (2008).

[36] C. Strauss, T. Takekoshi, F. Lang, K. Winkler, R. Grimm, J. Hecker Denschlag, and E. Tiemann, Phys. Rev. A **82**, 052514 (2010).

[37] J. Y. Seto, R. J. Le Roy, J. Vergès, and C. Amiot, J. Chem. Phys. **113**, 3067 (2000).

[38] A. J. Moerdijk, B. J. Verhaar, and A. Axelsson, Phys. Rev. A **51**, 4852 (1995).

[39] J. M. Hutson, M. Beyene, and M. L. González-Martínez, Phys. Rev. Lett. **103**, 163201 (2009).

[40] D. J. McCarron, H. W. Cho, D. L. Jenkin, M. P. Köppinger, and S. L. Cornish, Phys. Rev. A **84**, 011603 (2011).

[41] H. W. Cho, D. J. McCarron, D. L. Jenkin, M. P. Köppinger, and S. L. Cornish, Eur. Phys. J. D **65**, 125 (2011).

[42] Y.-J. Lin, A. R. Perry, R. L. Compton, I. B. Spielman, and J. V. Porto, Phys. Rev. A **79**, 063631 (2009).

[43] D. L. Jenkin, D. J. McCarron, M. P. Köppinger, H. W. Cho, S. A. Hopkins, and S. L. Cornish, Eur. Phys. J. D **65**, 11 (2011).

[44] P. A. Altin, N. P. Robins, R. Poldy, J. E. Debs, D. Döring, C. Figl, and J. D. Close, Phys. Rev. A **81**, 012713 (2010).

[45] M. Berninger, A. Zenesini, B. Huang, W. Harm, H.-C. Nägerl, F. Ferlaino, R. Grimm, P. S. Julienne, and J. M. Hutson, Phys. Rev. Lett. **107**, 120401 (2011).

[46] F. Ferlaino, S. Knoop, M. Mark, M. Berninger, H. Schöbel, H.-C. Nägerl, and R. Grimm, Phys. Rev. Lett. **101**, 023201 (2008).

[47] T. Weber, J. Herbig, M. Mark, H.-C. Nägerl, and R. Grimm, Science **299**, 232 (2003).

[48] A. L. Marchant, S. Händel, S. A. Hopkins, T. P. Wiles, and S. L. Cornish, Phys. Rev. A **85**, 053647 (2012).

[49] C. Chin, V. Vuletić, A. J. Kerman, S. Chu, E. Tiesinga, P. J. Leo, and C. J. Williams, Phys. Rev. A **70**, 032701 (2004).

[50] M. Berninger, A. Zenesini, B. Huang, W. Harm, H.-C. Nägerl, F. Ferlaino, R. Grimm, P. S. Julienne, and J. M. Hutson, arXiv:1212.5584.